Park, J., Lühr, H., Knudsen, D. J., Burchill, J. K., Kwak, Y.-S. (2017): Alfvén waves in the auroral region, their Poynting flux, and reflection coefficient as estimated from Swarm observations. - *Journal of Geophysical Research*, *122*, 2, pp. 2345—2360.

DOI: http://doi.org/10.1002/2016JA023527

AGU PUBLICATIONS

JGR

Journal of Geophysical Research: Space Physics

RESEARCH ARTICLE
10.1002/2016JA023527

Special Section:
Observations, Simulations, and Theory of Electric Currents in the Solar System

Alfvén waves in the auroral region, their Poynting flux, and reflection coefficient as estimated from Swarm observations

Jaeheung Park[1,2], Hermann Lühr[3], David J. Knudsen[4], Jonathan K. Burchill[4], and Young-Sil Kwak[1,2]

[1]Korea Astronomy and Space Science Institute, Daejeon, South Korea, [2]Department of Astonomy and Space Science, Korea University of Science and Technology, Daejeon, South Korea, [3]Helmholtz Centre Potsdam GFZ German Research Centre for Geosciences, Potsdam, Germany, [4]Department of Physics and Astronomy, University of Calgary, Calgary, Alberta, Canada

Key Points:
- Ionospheric reflection coefficients of Alfvén waves are estimated from Swarm measurements
- The ionospheric reflection coefficients are higher in summer than in winter, mostly peaking at the cusp and nightside auroral latitudes
- Poynting flux of the Alfvén waves is generally downward without notable hemispheric asymmetry in magnitudes

Correspondence to:
J. Park,
pj@kasi.re.kr

Citation:
Park, J., H. Lühr, D. J. Knudsen, J. K. Burchill, and Y.-S. Kwak (2017), Alfvén waves in the auroral region, their Poynting flux, and reflection coefficient as estimated from Swarm observations, *J. Geophys. Res. Space Physics*, *122*, 2345–2360, doi:10.1002/2016JA023527.

Received 7 OCT 2016
Accepted 25 JAN 2017
Accepted article online 30 JAN 2017
Published online 15 FEB 2017

Abstract The European Space Agency's Swarm constellation can measure electric field, magnetic field, and plasma density on board multiple satellites at altitudes of about 500 km. Based on the data set at high latitudes, we estimate Poynting flux and ionospheric reflection coefficients of Alfvén waves with scale sizes of about 10–100 km. The reflection coefficients are generally higher surrounding the cusp and auroral regions than in the polar cap and higher in the summer than in the winter hemisphere. In the summer (winter) hemisphere the reflection coefficients generally peak on the dayside (nightside). Distributions of the reflection coefficients are not controlled by those of in situ plasma density. Poynting flux of the Alfvén waves maximizes surrounding the cusp and near-midnight auroral region with magnitudes approaching 1 mW/m^2, which are consistent with previous magnetospheric observations. The observed Poynting flux is downward on average for both hemispheres, and the magnitudes do not exhibit clear hemispheric asymmetry.

1. Introduction

Shear Alfvén waves [e.g., *Alfvén*, 1942; *Lysak*, 1999; *Keiling*, 2009] are known to be the only magnetohydrodynamic (MHD) mode that can generate field-aligned currents [e.g., *Siscoe*, 1983; *Burke et al.*, 2016b, and references therein]. These waves can be reflected at the ionosphere due to the mismatch between the Alfvén conductance and that of the ionosphere. There have been many theoretical studies on Alfvén wave reflection by the ionosphere [e.g., *Knudsen et al.*, 1992; *Lysak*, 1993; *Vogt*, 2002; *Fedorov et al.*, 2016]. For the simplest case of reflection we may refer to the approach of *Burke et al.* [2016b, and references therein], which can be summarized as follows. For a freely traveling Alfvén wave (no reflection), the ratio of *E* field perturbation ($|\delta\vec{E}|$) and that of *B* field ($|\delta\vec{B}|$) equals to the local Alfvén velocity (V_A): $|\delta\vec{E}||\delta\vec{B}|^{-1} = V_A$. Any deviation of $|\delta\vec{E}||\delta\vec{B}|^{-1}$ from V_A can be interpreted as an indicator of reflection. When we assume (1) coplanarity between the incident and reflected waves and (2) plasma at the satellite altitude consists exclusively of oxygen ions, the ionospheric reflection coefficient of Alfvén waves can be estimated using *E* field, *B* field, and plasma density data from a satellite.

We may note that the reflection is more complex in the real ionosphere [e.g., *Vogt*, 2002; *Stasiewicz et al.*, 2000]. According to *Lessard and Knudsen* [2001], Alfvén waves with short perpendicular wavelength ($\lesssim$1 km) are not well reflected by the ionosphere (wavelength dependence). *Zhu et al.* [1993] showed that ionospheric irregularities can lead to field rotation of Alfvén waves, by which the coplanarity assumption mentioned above breaks down. *Haerendel* [2014] suggested that scale breaking of Alfvén waves results in maximum transport of energy from the magnetosphere to the ionosphere: so-called self-adjustment between Alfvénic and ionospheric conductance. According to *Shi et al.* [2013], not only normal ionospheric reflection but also electron/wave interactions can affect Alfvén waves.

Some of previous papers qualitatively interpreted their satellite/rocket observation results in terms of Alfvén wave reflection at the ionosphere. [see, e.g., *Knudsen et al.*, 1992; *Keiling et al.*, 2005; *Burke et al.*, 2016a]. However, only a few case studies have quantitatively estimated the reflection coefficients using real-world data, to the best of the authors' knowledge. *Knudsen et al.* [1992, equation (21)] estimated the impedance function of the ionosphere, which may be converted to reflection coefficient when Alfvén speed and the

distance from the reflection point are known. The impedance was estimated only for a few cases of real observations. *Burke et al.* [2016b] estimated the reflection coefficient from C/NOFS observations (*E* field, *B* field, and plasma density), but just for one case at a low L shell conjugate to Arecibo, Puerto Rico.

We have seen that no study has yet estimated the reflection coefficient using long-term in situ observations from low-Earth orbit satellites with global coverage. Hence, in this study we investigate the statistical distributions of reflection coefficient and Poynting flux of Alfvén waves at high latitudes including auroral/polar regions. In section 2 we briefly introduce the satellite, payload, and data processing methods. Section 3 presents the statistical results, which are discussed in depth in section 4. Finally, we summarize main findings of this study and draw conclusions in section 5.

2. Instruments and Data Processing Methods

2.1. Swarm Constellation

The Swarm constellation [e.g., *Olsen et al.*, 2013] consists of three satellites (Swarm-Alpha, Swarm-Bravo, and Swarm-Charlie) which were launched into a polar circular orbit at an altitude of about 500 km on 22 November 2013. During the first 2 months all the three satellites were in a string-of-pearls configuration. Afterward, intensive orbit maneuvers were conducted to put the satellites into the predetermined formation. Since 17 April 2014, when the formation was finalized, Swarm-Alpha and Swarm-Charlie fly at the same altitude around 450 km with latitudinal and longitudinal separation of about 0.5° and 1.4°, respectively [*Xiong et al.*, 2016, Figure 1]. The stand-alone satellite, Swarm-Bravo, has an orbit ~50 km higher than those of the paired Swarm-Alpha and Swarm-Charlie. Since April 2014 the orbit plane of Swarm-Bravo has gradually departed from those of the paired satellites with a speed of approximately 30° per year. Each satellite carries a Thermal Ion Imager (TII) for ion drift (or equivalently, *E* field) measurement, Vector Field Magnetometer and Absolute Scalar Magnetometer for *B* field observation, and Langmuir Probes (LPs) for diagnosing in situ plasma density.

In this study we use the 1 Hz magnetic field vectors (product identifier: MAG*x*_LR, where x denotes satellite identifiers of A, B, or C), 2 Hz *E* field vectors (product identifier: PREL_EFIx_TII1B), and 2 Hz plasma density (product identifier: PREL_EFIx_LP_1B). Due to the limited operation of the Swarm/TII [*Knudsen et al.*, 2014], from which the *E* field vectors are derived, we only use Swarm-Alpha and Swarm-Bravo data during the period between December 2013 and March 2015.

The data set is sorted into three seasons: combined equinox, June solstice, and December solstice. The combined equinox contains ±32 days around both 21 March and 21 September. June and December solstice seasons are defined as ±65 days around 21 June and 21 December, respectively. The length of each season (about 131 days) is approximately the minimum time span needed for a Swarm satellite to cover all local time sectors. Note that the data coverage of the Swarm/TII is poor in equinox and December [see *Park et al.*, 2016]. A single Swarm satellite did not provide data for all local times during each of those two seasons, leaving data gaps for part of the statistical bins.

Data obtained under geomagnetic disturbances are not discarded in this study because of the limited operation of the Swarm/TII. Note that the main body of Swarm/TII data originates from the period between 17 April and 30 September 2014. During that period the minimum *Dst* index is only −80 nT (http://omniweb.gsfc.nasa.gov/). That is, the whole period is relatively free of severe geomagnetic disturbances. The mean $F_{10.7}$ index during the period is about 136, and we consider that it is in the middle of the extended second peak of solar cycle 24.

2.2. Data Processing Scheme

The standard data products provide the *E* field and *B* field vectors in the North-East-Center (NEC) coordinate system. To obtain the direction of the background magnetic field, we first apply a low-pass Savitzky-Golay filter (order = 2, window size = 15 s ~110 km along the satellite track) to the *B* field data. The resultant background *B* field (hereafter, "mean magnetic field") is subtracted from the Swarm *B* field data to get the residual *B* field ($\delta\vec{B}$), which is considered to be due to Alfvén waves. The residuals are transformed into the mean-field-aligned (MFA) coordinates, where "*z*" is along the mean magnetic field, "*y*" is horizontal and toward magnetic east, and "*x*" completes the triad pointing toward outer L shells. Figures 1a and 1b present the residual *B* field in the meridional (*x*) and zonal (*y*) directions, respectively. Note that the mean magnetic field may be estimated

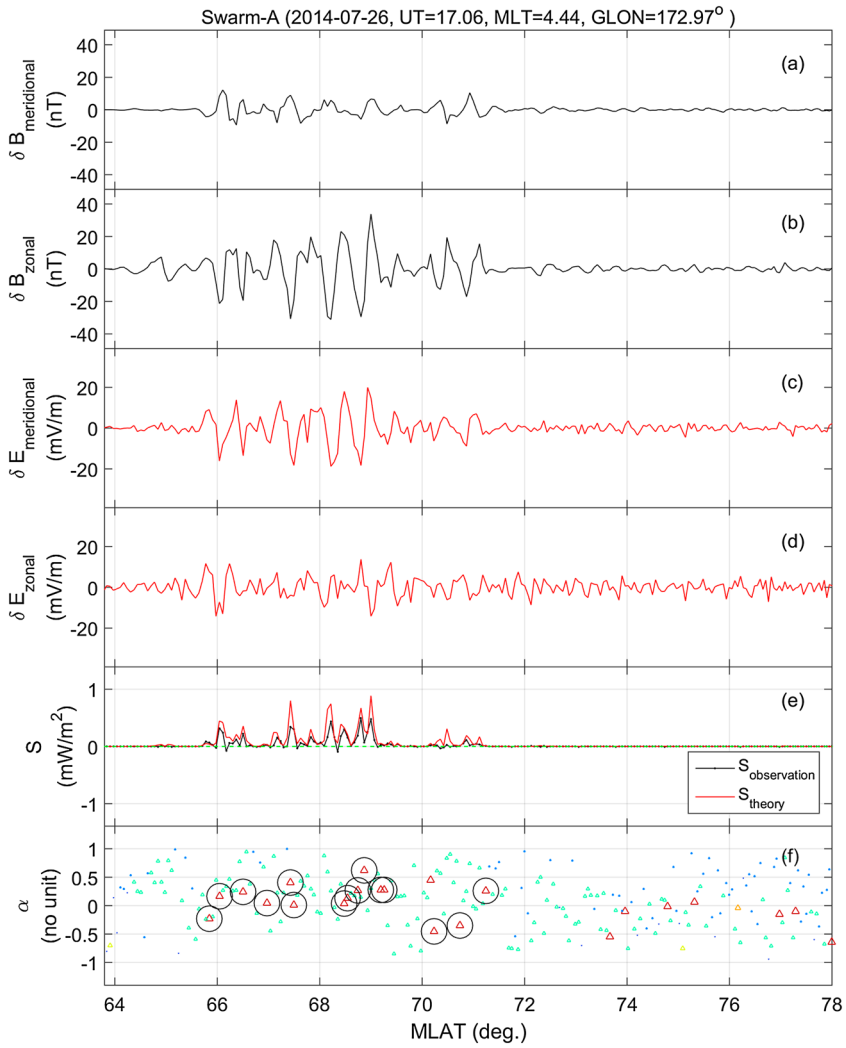

Figure 1. An example demonstrating how to estimate the ionospheric reflection coefficient using Swarm data: (a) δB_x (meridional residual B field), (b) δB_y (zonal residual B field), (c) δE_x (meridional residual E field), (d) δE_y (zonal residual E field), (e) Poynting flux parallel to the B field (black: calculated with $\delta\vec{E}$ and $\delta\vec{B}$ and red: estimated with $\delta\vec{B}$ assuming freely downward propagating Alfvén wave), and (f) ionospheric reflection coefficient. The UT, MLT, and GLON approximately correspond to the equatorial crossing of this southbound pass. See text for details.

from geomagnetic models: e.g., CHAOS-6 [*Finlay et al.*, 2016]. *Juusola et al.* [2016b] used such an approach. However, the Savitzky-Golay filtering is adopted in this study for the sake of consistency with the E field data processing, as will be described below.

To synchronize the different Swarm data sets, we resample the 2 Hz E field and 2 Hz plasma number density data at the time stamps of the 1 Hz B field data. Then, the same procedures (residual calculation and coordinate transformation) are applied to E field data in order to obtain the E field fluctuations coming from Alfvén waves ($\delta\vec{E}$). Figures 1c and 1d present the residual E field in the meridional (x) and zonal (y) directions in the MFA coordinate system, respectively. Considering the Nyquist frequency of 0.5 Hz (~15 km along the satellite track) and the window size of the Savitzky-Golay filter used for residual calculation (~110 km along the satellite track), the scale sizes of interest in this study can be considered approximately to be between 10 km and 100 km.

In this study we basically follow the approach of *Burke et al.* [2016b]. In addition to the residual E field ($\delta\vec{E}$) and residual B field ($\delta\vec{B}$), the third information, Alfvén velocity at the Swarm location is needed in order to calculate the ionospheric reflection coefficient. Assuming that the plasma at Swarm altitudes consists mostly of singly charged oxygen ions (O^+), the B field data and plasma number density (n_e) can be combined to yield Alfvén

velocity (V_A). Based on these three parameters ($\delta\vec{E}$, $\delta\vec{B}$, and V_A), we can estimate the ionospheric reflection coefficient (α) as follows (see *Burke et al.* [2016b, equations (2), (7), and (8)] for comparison):

$$S_z = \frac{\delta E_x\ \delta B_y - \delta E_y\ \delta B_x}{\mu_0} \tag{1}$$

$$K = \epsilon_0\ \left(\delta {B_x}^2 + \delta {B_y}^2\right)\ c^2\ V_A = \frac{1}{\mu_0}\left(\delta {B_x}^2 + \delta {B_y}^2\right)\ V_A \tag{2}$$

$$\alpha = \frac{K - |S_z|}{K + |S_z|}, \tag{3}$$

where μ_0 is the permeability, ϵ_0 is the permittivity, and c is the speed of light in vacuum. The S_z in equation (1) is the Poynting vector component along the mean magnetic field (MFA z-direction). The K parameter in equation (2) is similar to the P_m parameter in *Burke et al.* [2016b, equation (7)]. The former (K) is calculated from residual B field while the latter (P_m) from residual E field. The K becomes equal to $|S_z|$ if the Alfvén wave propagates freely without reflection: that is, if

$$|\delta\vec{E_{\text{perp}}}||\delta\vec{B_{\text{perp}}}|^{-1} = \left(\delta {E_x}^2 + \delta {E_y}^2\right)^{\frac{1}{2}}\left(\delta {B_x}^2 + \delta {B_y}^2\right)^{-\frac{1}{2}} = V_A \tag{4}$$

and

$$\delta\vec{E_{\text{perp}}} \cdot \delta\vec{B_{\text{perp}}} = (\delta E_x\ \delta B_x + \delta E_y\ \delta B_y) = 0, \tag{5}$$

where $\delta\vec{E_{\text{perp}}}$ and $\delta\vec{B_{\text{perp}}}$ are residual electric and magnetic fields perpendicular to the mean magnetic field (i.e., residual fields on the MFA x-y plane). The α in equation (3) is equivalent to that in *Burke et al.* [2016b, equation (8)] and obtained by rearranging the terms in *Burke et al.* [2016b, equations (2) and (5)]. When $\alpha = +1$, the reflected E field becomes antiparallel to the incident E field with equal magnitude (i.e., E field sign reversal) so that the sum of incident and reflected E field leads to zero net E field. Simultaneously, the reflected B field is parallel to the incident B field with equal magnitude, which leads to net B field doubled in magnitude. If $\alpha = -1$, on the contrary, the net E field becomes doubled, while the net B field disappears. Zero value of α signifies freely propagating Alfvén wave without reflection.

There are several conditions that each data point should satisfy to be qualified to generate a valid reflection coefficient. First, we avoid regions of geographic latitude (GLAT) poleward of ±84°. As the NEC coordinate system is based on geographic coordinate axes, the "north" and "east" coordinate axes vary rapidly when a satellite crosses near the pole. Because we calculate the mean magnetic field by Savitzky-Golay-filtering the B field data in the NEC frame, regions close to the geographic poles may exhibit rapid variation of residual B field components. As the orbit inclination angles of the Swarm satellites are about 87°–88°, only a small portion of data is discarded by this criterion ($|\text{GLAT}| \leq 84°$). Second, data points for which δB_x, δB_y, or δB_z is larger than 400 nT are discarded. Third, either δB_x or δB_y should have a magnitude of ≥0.4 nT in order to avoid misinterpreting instrument noise.

Following *Burke et al.* [2016b], we impose two more conditions for data selection. As for the fourth condition, the magnitude of Poynting flux along the mean magnetic field (S_z) calculated from $\delta\vec{E}$ and $\delta\vec{B}$ (black curve in Figure 1e) should be larger than some thresholds. This threshold is set to 1 μW/m^2, considering *Burke et al.* [2016b, Figure 2]. This threshold is shown as green dashed horizontal line in Figure 1e but cannot be distinguished from the zero level due to the small value (note that the ticks on the vertical axis in Figure 1e are given every 1000 μW/m^2). The red curve in Figure 1e represents the Poynting flux estimated from $\delta\vec{B}$ and V_A under the assumption of $\left(\delta {E_x}^2 + \delta {E_y}^2\right)\left(\delta {B_x}^2 + \delta {B_y}^2\right)^{-1} = V_A^2$: freely downward propagating Alfvén wave. Under this assumption we can calculate the Poynting flux without E field data: this value will be discussed in depth later. As the fifth condition, in order to avoid the influence of rotation of E field or B field after ionospheric reflection [*Zhu et al.*, 1993], we discard data points where the angle between $\delta\vec{E}$ and $\delta\vec{B}$ is smaller than $\cos^{-1}(0.2) \sim 78°$.

Considering the suboptimal quality of the Swarm E field data, we impose the sixth condition for data selection. For every data point of reflection coefficient, the correlation coefficient either between δE_x and δB_y or between δE_y and δB_x (over 11 values centered at the data point of interest) should be larger than 0.4 in magnitude.

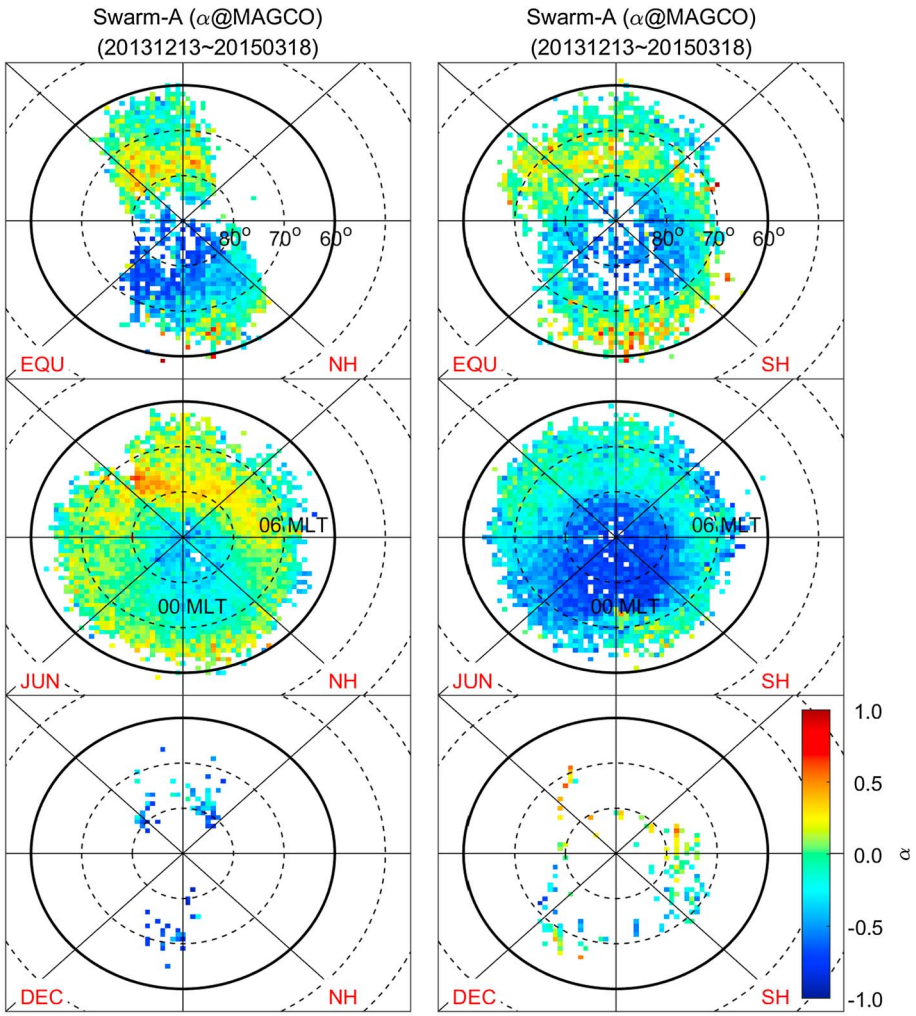

Figure 2. Distribution of ionospheric reflection coefficients as a function of MLAT and MLT, which are based on Swarm-Alpha observations. Concentric circles are given every 10° in MLAT. Top and bottom inside each panel signify 1200 MLT and 0000 MLT, respectively. Each row represents a season (combined equinox, June solstice, and December solstice), while the left and right columns correspond to the Northern and Southern Hemispheres, respectively. The reddish colors represent positive reflection coefficients while the bluish ones negative.

In this way we can minimize the effect of instrument noise that may dominate the Swarm/TII data occasionally [e.g., *Knudsen et al.*, 2014].

The reflection coefficients (α) are calculated only for data points passing all the criteria mentioned above. In Figure 1f the bluish small symbols represent data points which satisfy few conditions mentioned above, and the color changes toward red as the number of satisfied conditions increase. Fully qualified data points are highlighted by black circles surrounding brown triangles.

Note that although we use the approach of *Burke et al.* [2016b], our method addresses the issues raised by *Lessard and Knudsen* [2001] and *Zhu et al.* [1993]. As we use 1 Hz data of Swarm, the distance between two adjacent data points is about 7.5 km (considering the satellite speed of 7.5 km/s). Then, the total penetration of small-scale (wavelength $\lesssim$1 km) Alfvén waves through the ionosphere, as mentioned in *Lessard and Knudsen* [2001], is not relevant to this study. Similarly, our results are mostly free from Alfvén wave dispersion because the dispersion effect becomes significant when the transverse scale is less than 10 km [*Chaston et al.*, 2007]. Finally, the angle between $\delta\vec{E}$ and $\delta\vec{B}$ is kept larger than $\cos^{-1}(0.2) \sim 78°$, so that possible field rotation by ionospheric irregularities is avoided [e.g., *Zhu et al.*, 1993].

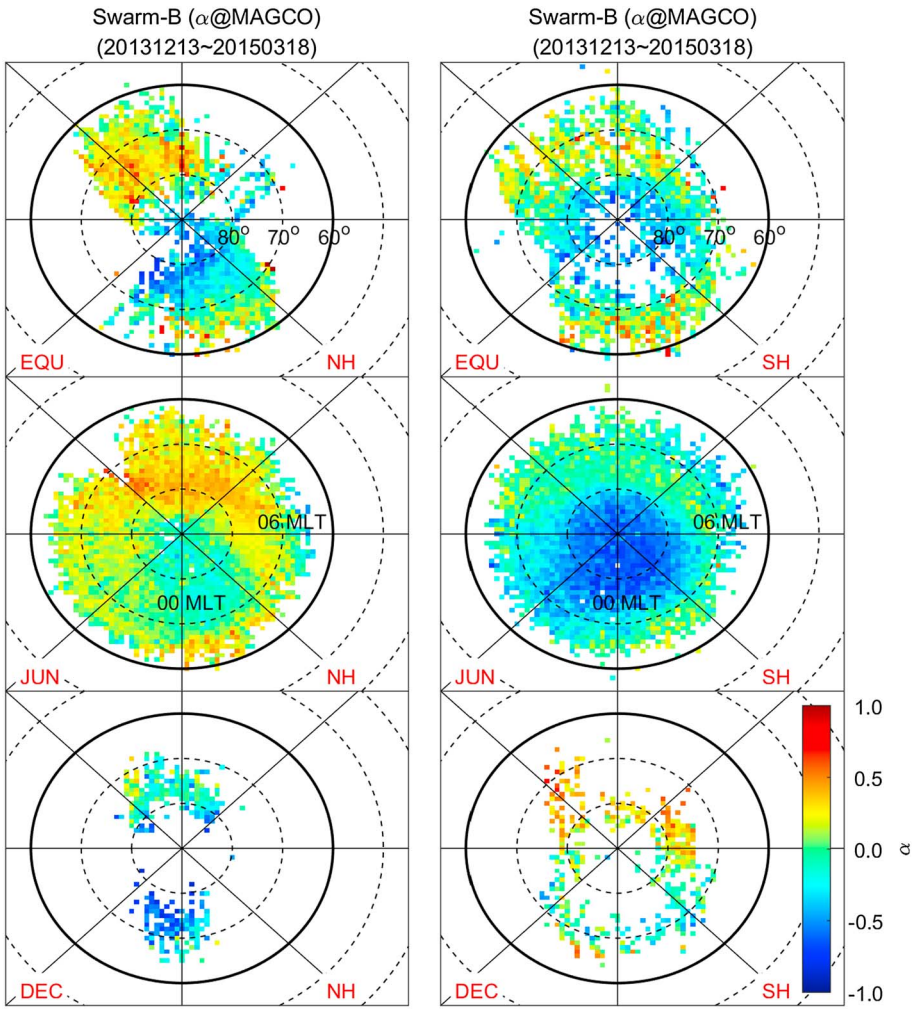

Figure 3. The same as Figure 2 but for Swarm-Bravo.

3. Statistical Results

3.1. Ionospheric Reflection Coefficients

Figure 2 presents the distribution of ionospheric reflection coefficients (α) derived from the Swarm-Alpha data. In Figure 2 the left and right columns correspond to the Northern Hemisphere (NH) and the Southern Hemispheres (SH), respectively. Each row represents a season: from top to bottom combined equinox, June solstice, and December solstice, as defined in section 2. The center of the concentric circles is the magnetic pole of the respective hemisphere, and circles are given every 10° in magnetic latitude (MLAT). The azimuth angles represent magnetic local time (MLT): noon is toward the top of each panel, and dawn/dusk are to the right/left. The space in each panel is segmented into square bins of 1° × 1° in MLAT, to each of which one color is assigned. The color signifies ionospheric reflection coefficient (α): red is positive and blue is negative. Only the bins containing ≥10 data points are shown in the figure. Note that the data coverages during combined equinoxes and December solstice are incomplete due to the limited operation time of Swarm/TII during those seasons and because of the *E* field noise issue around December 2013 [*Knudsen et al.*, 2014]. Figure 3 is the same as Figure 2 but for Swarm-Bravo. Figure 3 generally agrees with Figure 2 in many aspects as addressed below.

First, we discuss the summer-winter asymmetry in Figures 2 and 3. During June solstice (Figures 2 and 3, middle rows) the reflection coefficients are generally larger in the summer (northern) hemisphere than in the winter (southern) hemisphere, especially on the dayside. This hemispheric asymmetry can also be identified during December solstice (Figures 2 and 3, bottom rows) in spite of the poor data coverage. During the combined equinox, the reflection coefficients do not exhibit conspicuous hemispheric asymmetry.

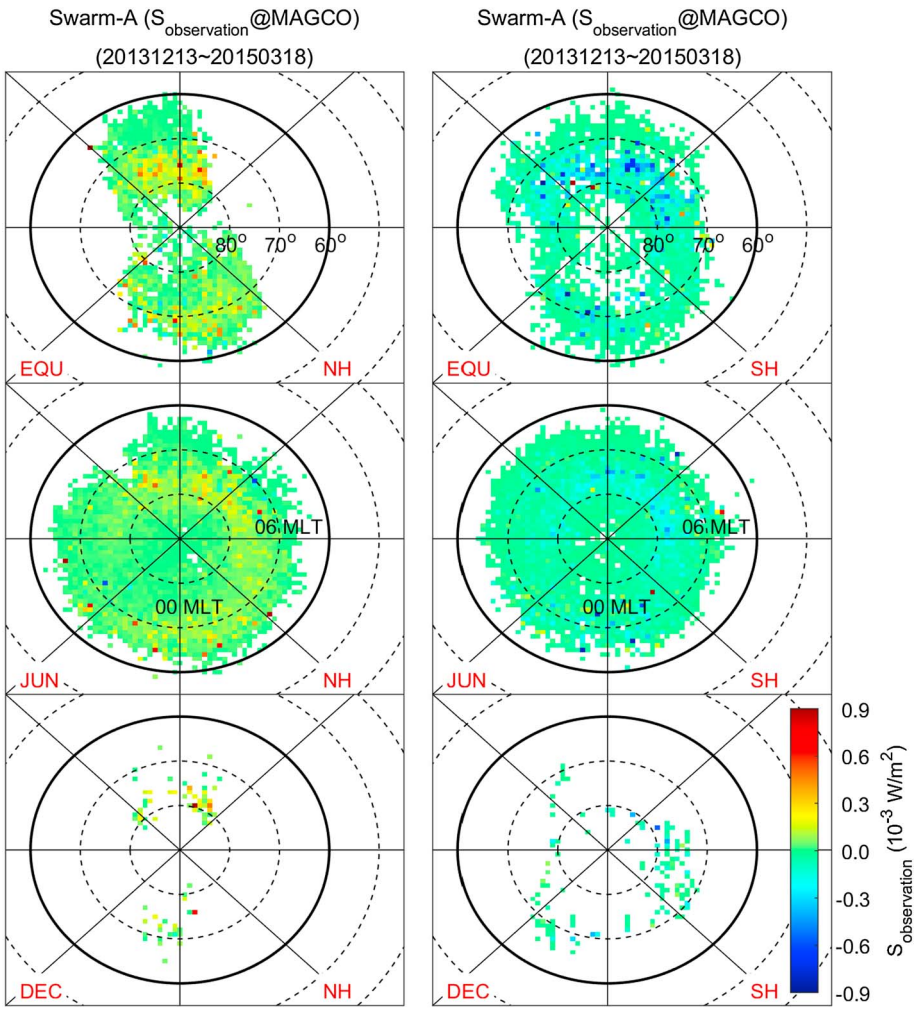

Figure 4. The same as Figure 2 but presenting Poynting flux component along *B* field (S_z) estimated from *E* field and *B* field data of Swarm-Alpha. The reddish colors represent parallel Poynting flux (downward in the NH) while bluish colors antiparallel (downward in the SH).

Next, we discuss the MLAT-MLT dependences in Figures 2 and 3. The reflection coefficients in the polar cap (|MLAT| > 80°) are generally negative or at least lower than at auroral regions (60 ≤ |MLAT| ≤ 80°). As for the MLT dependence during June solstice, (1) the summer (northern) hemisphere exhibits generally more positive reflection coefficients on the dayside than on the nightside, and (2) the winter (southern) hemisphere exhibits primarily negative reflection coefficients except for the auroral oval with a weak peak in the nighttime (postmidnight) sector. Unfortunately, the MLT dependence cannot be seen easily in December solstice due to incomplete data coverage. During the combined equinox the reflection coefficients do not exhibit conspicuous day-night asymmetry

3.2. Poynting Flux and In Situ Plasma Density

Figures 4 and 5 have the same format as Figures 2 and 3 but present the Poynting flux component along *B* field (S_z), as calculated by equation (1). Note that only the data points qualified for Figures 2 and 3 are plotted in Figures 4 and 5. Positive Poynting flux (red color) represents field-aligned direction of energy flow (downward in the Northern Hemisphere). Negative values (blue color) correspond to the direction antiparallel to the *B* field (downward in the Southern Hemisphere). In Figures 4 and 5 the following two points are immediately clear. First, significant (large-magnitude) Poynting flux appears in dayside regions surrounding the cusp (MLT ~ 1200 and |MLAT| ~ 75°) and near-midnight aurora region (MLT ~ 0000 and |MLAT| ~ 70°). Second, the peak magnitude of the Poynting flux is about 1 mW/m^2, without conspicuous hemispheric asymmetry (e.g., summer-winter difference in Poynting flux magnitude). Third, the strong Poynting flux is mainly downward in both hemispheres.

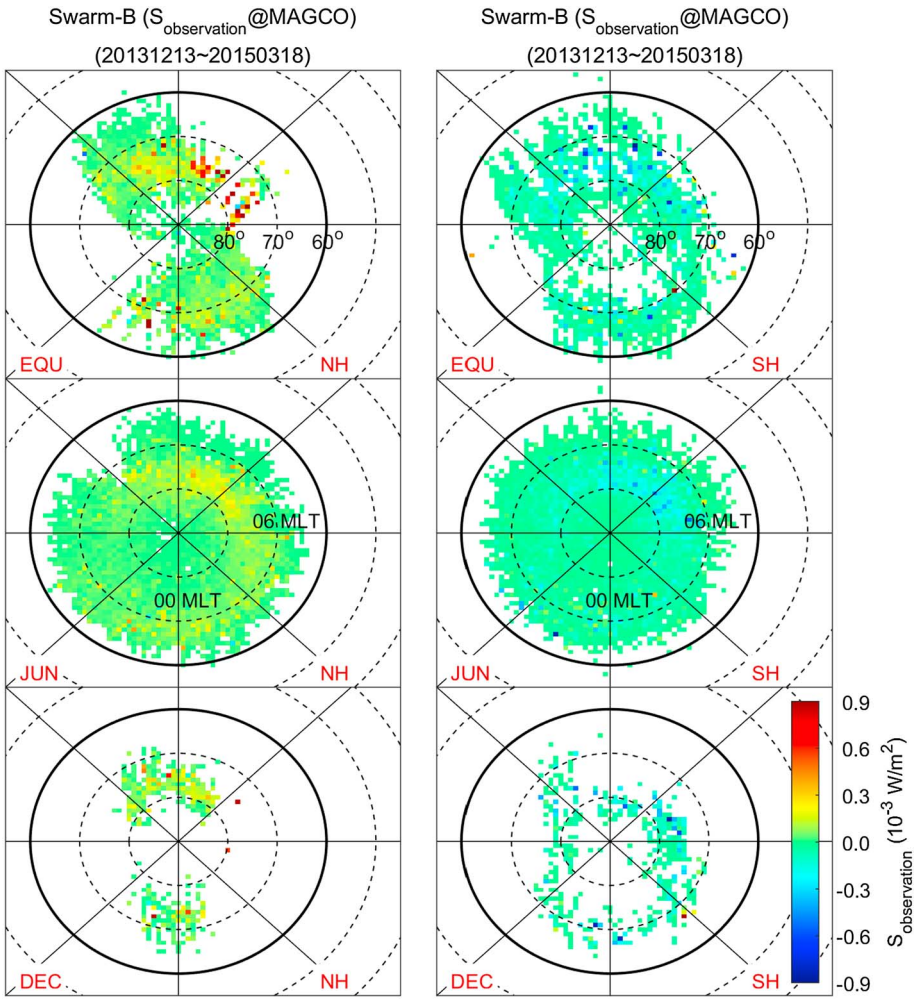

Figure 5. The same as Figure 4 but for Swarm-Bravo.

Figures 6 and 7 are the same as Figures 4 and 5, but the Poynting flux is estimated without *E* field data. Assuming freely downward propagating Alfvén waves, with the help of equations (4) and (5) we have

$$S_z = \frac{\sqrt{\delta B_x^2 + \delta B_y^2}\sqrt{\delta E_x^2 + \delta E_y^2}}{\mu_0} = \frac{\left(\delta B_x^2 + \delta B_y^2\right) V_A}{\mu_0} = \left(\delta B_x^2 + \delta B_y^2\right) \frac{B_0}{\mu_0 \sqrt{n_e \mu_0 m_{ion}}}, \quad (6)$$

where B_0 and n_e are the *B* field strength and plasma number density data from Swarm, respectively. The m_{ion} is the mass of ionospheric ions. Note that the Poynting flux from equation (6) is equivalent to the *K* parameter in equation (2). Assuming that the plasma at Swarm altitudes consists mostly of singly charged oxygen ions (O^+), we can estimate the Poynting flux without counting on *E* field measurements. The purpose of showing these figures is to check whether *B* field data from a satellite that cannot reliably measure *E* field may also be exploited to estimate Poynting flux. Note that this method produces positive definite values of Poynting flux without directional information. The direction of the Poynting flux is assumed to be downward, i.e., parallel to the mean magnetic field in the NH and antiparallel in the SH. Note also that only those data points qualified for Figures 2 and 3 are plotted in Figures 6 and 7. The MLAT-MLT distributions in Figures 6 and 7 generally agree with those of Figures 4 and 5, except that the peak at the nighttime auroral region in the NH during June solstice is not so conspicuous. The most notable feature of Figures 6 and 7 is that the magnitudes of Poynting flux are more than two times larger than in Figures 4 and 5. For Swarm-Alpha the total sum of magnitudes of the observed Poynting flux shown in Figure 4 is only 44% of that of Figure 6. For Swarm-Bravo the total sum

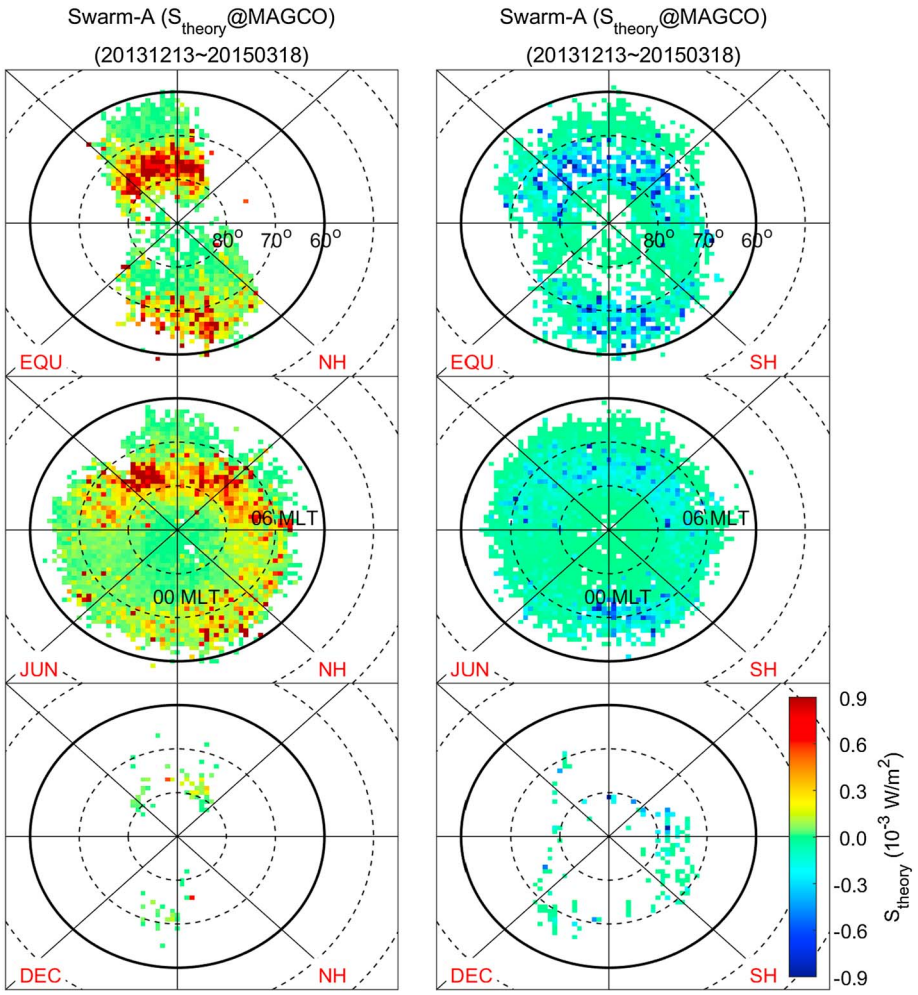

Figure 6. The same as Figure 4 but presenting Poynting flux component along *B* field (S_z) estimated solely from *B* field data of Swarm-Alpha, assuming freely downward propagating Alfvén wave. The reddish colors represent parallel Poynting flux (downward in the NH) while bluish colors antiparallel (downward in the SH).

of magnitudes of the observed Poynting flux shown in Figure 5 is only 32% of that of Figure 7. That is, the Poynting flux estimated without *E* field is generally ~3 times larger in magnitude than that from both *E* field and *B* field data.

Figures 8 and 9 present maps of in situ plasma density measured by the LPs on board Swarm-Alpha and Swarm-Bravo, respectively. Note that only those data qualified for Figures 2 and 3 are plotted in Figures 8 and 9. Generally, the density is higher on the dayside than on the nightside and higher in summer than in winter. The statistical distributions of the in situ plasma density do not agree well with the maps of ionospheric reflection coefficients in Figures 2 and 3. The results will be discussed further in section 4.

4. Discussion

In this study we have investigated the statistical properties of medium-scale Alfvén waves (approximately 10–100 km) in the ionosphere (altitudes of ~500 km). The availability of electric and magnetic field measurements allows to determine important electromagnetic characteristics.

4.1. Ionospheric Reflection: Reality or Artifact?

In section 3 we found difference of a factor of 3 between (1) the magnitudes of the Poynting flux calculated from actual Swarm *E* field and *B* field measurements ($|S_z|$) and (2) that estimated without *E* field data assuming freely propagating downward Alfvén wave (the *K* parameter in equation (2)). The difference can be interpreted

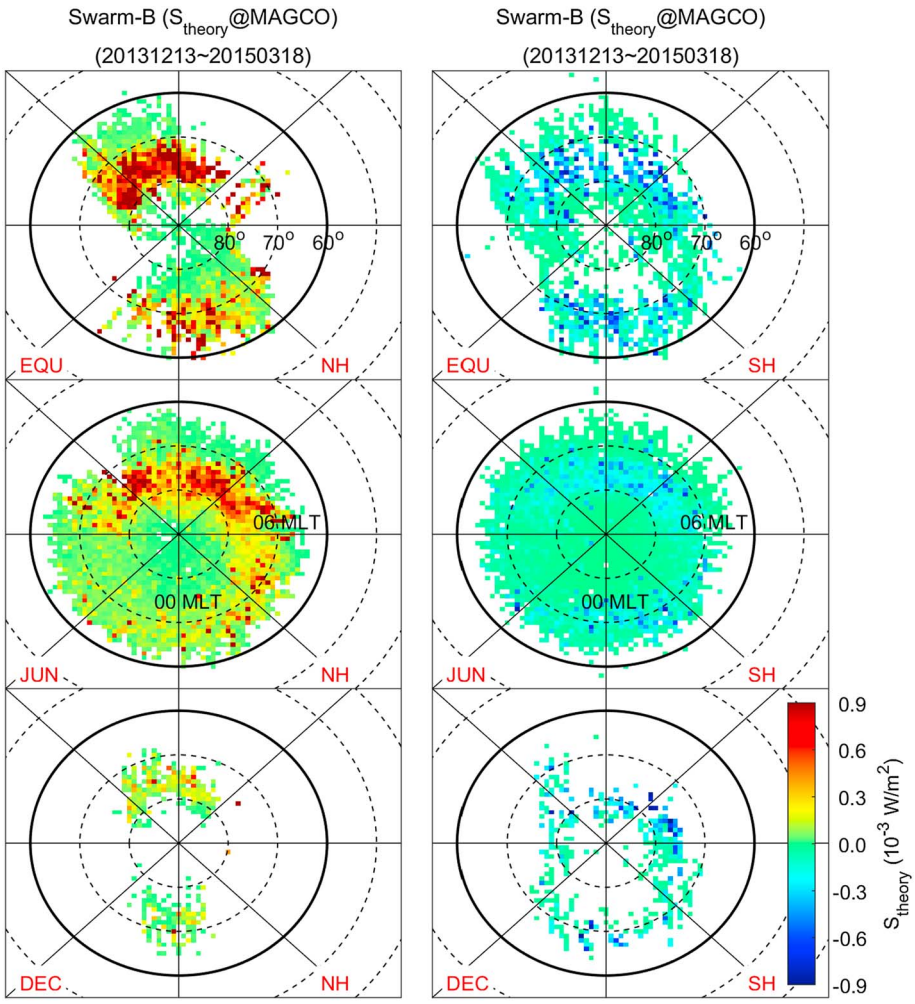

Figure 7. The same as Figure 6 but for Swarm-Bravo.

as reflection of Alfvén waves at the ionosphere. When the ratio between $|K|$ and $|S_z|$ is unity, for example, equation (3) leads to zero reflectance of the ionosphere.

Given a number of quality issues of the Swarm/TII [*Knudsen et al.*, 2014], one may suspect that $\delta\vec{E}$ from Swarm be systematically underestimated in magnitude, which may have resulted in the "factor-of-3" difference. According to *Fiori et al.* [2016], however, plasma drift velocity (or equivalently, *E* field) measured by Swarm/TII exhibits reasonable correlation with statistical convection models when bias levels are properly considered: see also *Knudsen et al.* [2017]. Furthermore, the Swarm/TII data slightly "over"estimate plasma drift [*Fiori et al.*, 2016, Figure 5]. Hence, the factor of 3 difference in our study cannot be due to systematic "under"estimation of Swarm/TII.

As plasma density is needed in Alfvén speed calculation, the absolute accuracy of n_e may be another error source. According to *Pedatella et al.* [2015], the LP consistently underestimates plasma density by about 8–15%. However, this amount cannot explain the Poynting flux difference by a factor of 3 because only the square root of n_e contributes to the Alfvén velocity, see equation (6). Even 20% underestimation of n_e (see also *Knudsen et al.* [2017]) leads only to 10% overestimation of Poynting flux.

The assumption of pure O^+ plasma in V_A calculation should also be checked. At intervals where strong ion heating occurs (mainly at high latitudes) the ion composition at Swarm altitudes can differ significantly from pure O^+. NO^+ can be present, for example, in which case the theoretical Poynting flux (*K*; calculated without *E* field data) would be an overestimate. This could explain a small part of the factor of 3 difference in theoretical versus observational Poynting flux. However, even under an extreme assumption that the ionospheric plasma

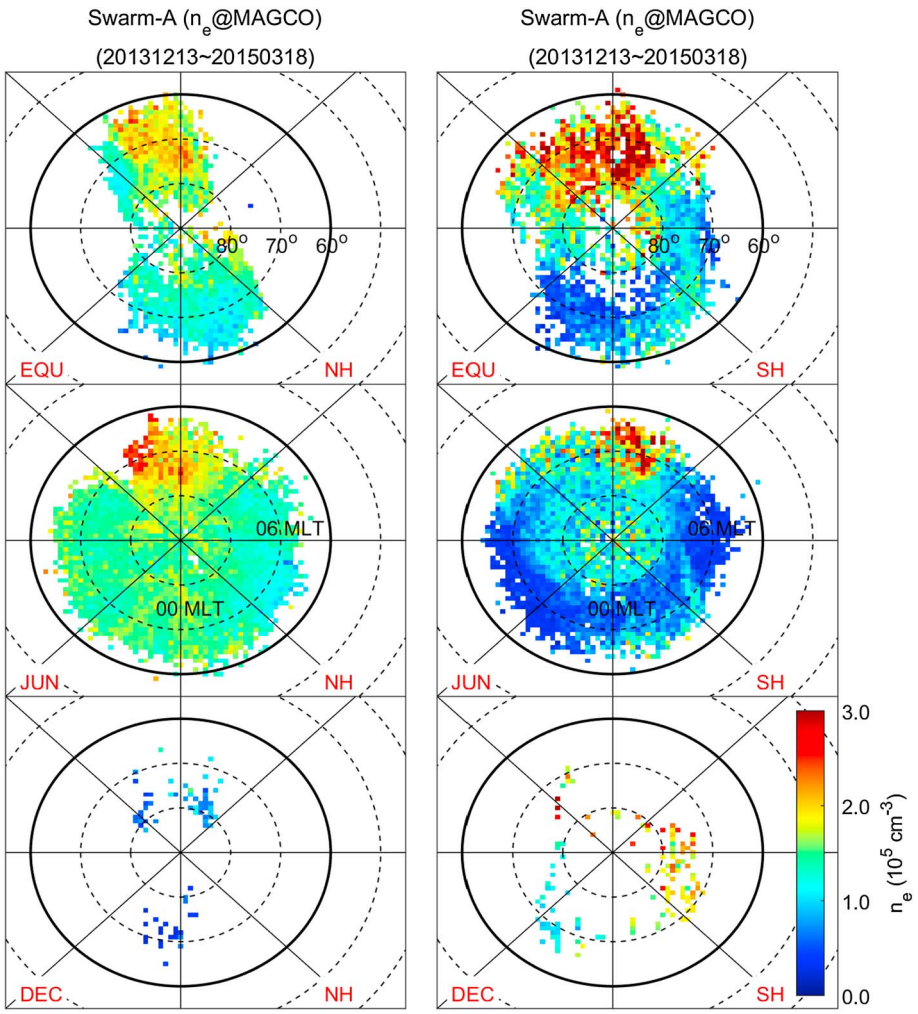

Figure 8. The same as Figure 2 but showing in situ plasma density measured by the LP on board Swarm-Alpha.

at Swarm altitudes consists purely of NO^+, the Poynting flux ratio between plasma of O^+ and that of NO^+ (see equation 6) is $\sqrt{(16+14)/16} \sim 1.37$, which is still insufficient to explain the factor of 3.

Therefore, we suggest that the main reason for the factor of 3 overestimation is the fact that the ionospheric reflection coefficient is generally nonzero. Hence, we will discuss the ionospheric reflection in depth in the following sections.

4.2. Ionospheric Reflection Coefficient and Pedersen Conductance

To first order the ionospheric reflection coefficient (α) is positively correlated with the ionospheric Pedersen conductance when a fixed Alfvén conductance is assumed. According to *Burke et al.* [2016a, equation (3)] (note their opposite sign convention),

$$\alpha = \frac{\Sigma_{PR} - \Sigma_{AR}}{\Sigma_{PR} + \Sigma_{AR}}, \tag{7}$$

where Σ_{PR} is the Pedersen conductance of the ionosphere and $\Sigma_{AR} = (\mu_0 V_A')^{-1}$, where V_A' is the Alfvén velocity at the ionospheric reflection layer. According to this equation, the reflection coefficient of −1 and +1 can be reached when ionospheric Pedersen conductance (Σ_{PR}) is much smaller and larger than Alfvén conductance (Σ_{AR}), respectively. When the two conductance values match perfectly, α becomes zero. That is, a poorly conducting ionosphere leads to negative α, while highly conductive ionosphere results in positive α.

Although equation (7) may be oversimplification, in particular, for Alfvén waves with small spatial scales, it would still be enlightening to compare our reflection coefficients with previous papers on ionospheric Pedersen conductance. Therefore, in this subsection we qualitatively compare the α values in Figures 2

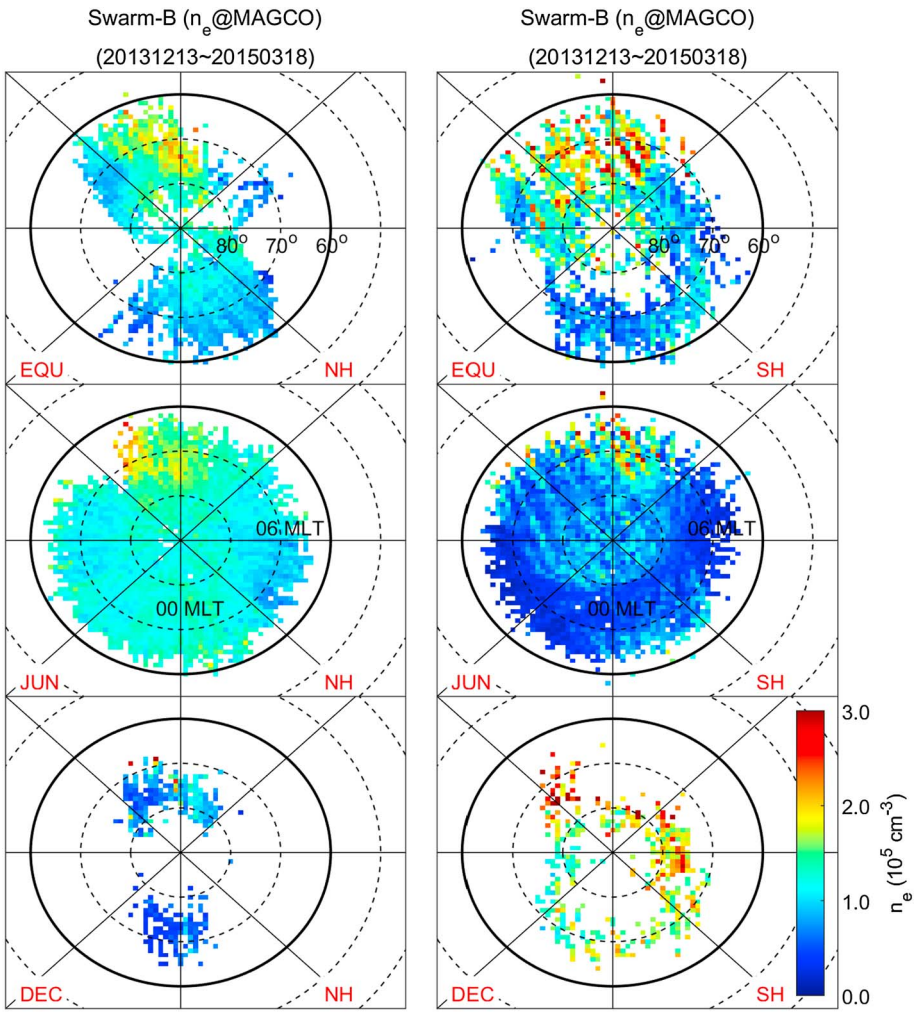

Figure 9. The same as Figure 8 but for Swarm-Bravo.

and 3 with the conductance maps reported in previous studies. Note also that most of previous studies on ionospheric Pedersen conductance using real-world data [e.g., *Aikio et al.*, 2012] had limited spatial and/or temporal coverage [see *Juusola et al.*, 2016b, and references therein].

In the summer hemisphere our results are roughly consistent with the Pedersen conductance models of *Ridley* [2007, Figure 4], *Ridley et al.* [2004] (Plate 13), and *Juusola et al.* [2014, Figures 9d–9f] in that the reflection coefficient (or Pedersen conductance) is generally higher on the dayside than on the nightside. However, the reflection coefficients on the summer dayside (Figures 2 and 3) do not monotonically increase with decreasing |MLAT|, while the Pedersen conductance in the above mentioned models does.

In the winter hemisphere the peak of the reflection coefficients (Figures 2 and 3) appears in the postmidnight sector, which is consistent with the Pedersen conductance distribution in *Ridley* [2007, Figure 4], *Ahn et al.* [1998] (Plate 1), and *Cousins et al.* [2015, Figure 2]. Our result also agrees with a case study reported by *Green et al.* [2007, Figure 9] in that the wintertime peak of Pedersen conductance exists around the midnight MLT. The postmidnight peak in our study appears to be related to diffuse auroral precipitations [e.g., *Newell et al.*, 2009, Figure 5]. However, a minimum in reflection coefficient exists in the premidnight sector in our results while the papers mentioned above have the minimum Pedersen conductance in the postnoon region.

In equinox, in spite of the incomplete data coverage, the overall reflection coefficients appear slightly higher than (or comparable to) the solstitial values. This result is at odds with *Ridley* [2007, Figure 4] and *Ridley et al.* [2004] (Plates 10, 12, and 13), where local summer exhibits Pedersen conductance higher than the equinoctial ones.

In summary, the reflection coefficients in Figures 2 and 3 generally agree with previous studies of ionospheric Pedersen conductance but exhibit discrepancy for some details. There may be multiple reasons for these discrepancies because both our method and previous models have their own limitations. Nonnegligible noise in Swarm *E* field data [*Knudsen et al.*, 2014], if having escaped serendipitously from our selection criteria (see section 2), may contaminate Figures 2 and 3. Especially, when the *E* field noise appears at subauroral regions (very weak $\delta\vec{B}$, by definition), the strong *E* field (noise) and weak *B* field result erroneously in a low reflection coefficient (e.g., decreasing in a direction from +1 toward −1) [*Burke et al.*, 2016b, p. 4926]. This may be a reason that the reflection coefficients on the summer dayside do not increase monotonically with decreasing |MLAT| but are saturated or slightly weakened at the subauroral latitudes. Small (i.e., more negative) values of alpha roughly correspond to very small ionospheric Pedersen conductance, as stated in a preceding paragraph. It may be one of the reasons for the discrepancy between our reflection coefficients and Pedersen conductance in, for example, *Ridley* [2007, Figure 4]. The noise issue of the Swarm/TII instrument is not easy to resolve solely by data processing methods. Though we have tried the best to avoid the noise as described in section 2, further studies which use longer-term and higher-precision electric field observations than this study are warranted.

4.3. Poynting Flux and In Situ Plasma Density

Features in Figures 4 and 5 may be summarized by the following two statements. First, strong Poynting flux appears in dayside regions surrounding the cusp and near-midnight aurora region with peak magnitudes approaching 1 mW/m^2. Note that we have filtered out data points which do not conform to colinear reflection of Alfven waves (see section 2.2). Hence, the Poynting flux in this study may be a conservative estimate of that actually impinging onto the ionosphere. Second, the strong Poynting flux is mainly directed toward the ground in both hemispheres. These two results generally agree with the 1 year Polar satellite observations presented by *Keiling et al.* [2003] and with the Lyon-Fedder-Mobarry simulations by *Zhang et al.* [2012, Figure 1]. The qualitative agreement supports that the results in our study are representative of Alfvén waves existing in the magnetosphere. It is furthermore interesting to note that the regions of strong small-scale Poynting flux generally agree with source regions of cold ion outflow (for $Dst < -20$ nT) [*Li et al.*, 2012, Figure 3].

Figures 6 and 7 presented Poynting flux magnitude estimated solely with $\delta\vec{B}$ data under the assumption of freely downward propagating Alfvén waves. When compared to Figures 4 and 5, Poynting flux magnitude in Figures 6 and 7 is higher by approximately 3 times. The overestimation is also evident in the example given in Figure 1e: compare the black and red curves. According to *Burke et al.* [2016b, p. 4926] the reflection coefficient (α) is generally positive. Actually, our Figures 2 and 3 exhibit positive values of reflection coefficient (α) for regions of strong Poynting flux (Figures 4 and 5). To recapitulate, the positive values of reflection coefficient (α) have the following effects: (1) the incident and reflected $\delta\vec{E}$ values are in antiphase and (2) the incident and reflected $\delta\vec{B}$ values are in phase. Hence, the ionospheric reflection leads to reduction of observed (net) $\delta\vec{E}$ and enhancement of observed (net) $\delta\vec{B}$. This may be one reason that Figures 6 and 7, which are solely based on observed (net) $\delta\vec{B}$ data and Alfvén speed, present Poynting flux higher in magnitude than Figures 4 and 5. The range of horizontal wavelengths in this study (approximately 10–100 km) may still be too large for the approach counting on *B* field and Alfvén velocity to give reliable results. It is consistent with *Lessard and Knudsen* [2001], who showed that Alfvén waves with wavelengths shorter than 1 km are not well reflected by the ionosphere.

The maps of plasma density measured by the LP on board Swarm-Alpha and Swarm-Bravo (Figures 8 and 9) do not match well with the maps of ionospheric reflection coefficient (Figures 2 and 3). Considering that the reflection coefficient is positively correlated with ionospheric conductance (see equation (7)), its mismatch with the in situ plasma density, which should be proportional to local Pedersen conductivity, is notable. The mismatch suggests that the ionospheric conductance is dominated not by the *F* region topside ionosphere but by the *E* region conductivity. The ion-neutral collision frequency is low in the *F* region for making significant contributions to the conductance. Figures 2 and 3 (ionospheric reflection coefficient) appear similar to the Pedersen conductivity per gas density in *Kwak and Richmond* [2007, Figure 1] (denoted as λ_1 in their equation (7)): especially at 123 km and 142 km altitudes. The agreement implies that ionospheric Pedersen conductance (integrated Pedersen conductivity along *B* field) may be dominated by the conductivity around the 123 km and 142 km altitudes, which is far below the Swarm altitudes.

4.4. Methodological Comparisons With Other Studies

In this subsection we briefly mention a number of previous papers where similar methods as in this study (and in *Burke et al.* [2016b]) were used. *Ishii et al.* [1992] calculated the ratio between $\delta B_{\text{north-south}}$ and $\mu_0\ \delta E_{\text{east-west}}$ measured by the Dynamics Explorer 2 (DE 2) satellite and showed that the ratio generally agrees with ionospheric Pedersen conductance calculated by the International Reference Ionosphere-86 model. The agreement is good for larger scales (64–256 km), which confirms the theoretical expectation of *Kelley et al.* [1991, equation (1)], while it is compromised for scales smaller than 16 km. By rearranging equations of *Burke et al.* [2016b, p. 4927], we can show that $\Sigma_{\text{PR}} = (1+\alpha)(1-\alpha)^{-1}(\mu_0 V_A')^{-1}$. Hence, if we know (1) V_A', which is the Alfvén velocity at the ionospheric reflection layer, and (2) $(\delta B_{\text{north-south}})(\mu_0\ \delta E_{\text{east-west}})^{-1}$, which *Ishii et al.* [1992] showed to be equivalent to Σ_{PR} for larger scales (64–256 km), the ionospheric reflection coefficient (α) can be directly calculated. Therefore, the methodology of *Ishii et al.* [1992] is similar to ours although the reflection coefficients were not explicitly calculated by *Ishii et al.* [1992].

Second, *Juusola et al.* [2016a] demonstrated a way to estimate ionospheric conductance using Swarm *E* field and *B* field data via the Spherical Elementary Current Systems method. In a nutshell, the method first calculates *E* region perpendicular current density from *B* field data and divides it by the *E* field data (measured by satellites) to obtain the ionospheric conductance. A similar method was used by *Green et al.* [2007], while their *E* field data were obtained by the Super Dual Auroral Radar Network. Compared with our method (and that of *Burke et al.* [2016b]), that of *Juusola et al.* [2016a] has the following merits: (1) no plasma density data are needed and (2) both Pedersen and Hall conductance can be calculated (our method calculates the ionospheric reflection coefficient, from which only the Pedersen conductance can be approximated). On the other hand, the deficiency of their method is as follows: (1) the most general form of their method aims at large horizontal scale length ($\geq$200 km) and (2) complex fitting, gridding, and decomposition into divergence-free, curl-free, and field-aligned currents are needed. Note that the possibility of conductance estimation was only mentioned by *Juusola et al.* [2016a]. The method was actually applied to real Swarm data in *Juusola et al.* [2016b], but just for one case of an auroral arc. Our approach and that of *Juusola et al.* [2016a, 2016b] can be deemed complementary to each other, and global comparison of their results in the future is highly warranted.

Third, *Lühr et al.* [2014] analyzed the 50 Hz $\delta\vec{B}$ data measured by the Challenging Minisatellite Payload (CHAMP) satellite around equatorial plasma bubbles (EPBs). They estimated unmeasured $\delta\vec{E}$ under the assumption of freely propagating Alfvén waves (i.e., no reflection from the ionosphere, according to *Burke et al.* [2016a, p. 2578]). Note that this method is similar to that used for our Figures 6 and 7. Because neither $\delta\vec{E}$ nor ionospheric reflection coefficient (α) was available to *Lühr et al.* [2014], the approach may have been the best trial they could do with the CHAMP data. Their assumption of freely propagating Alfvén waves may be justified by the argument of *Lessard and Knudsen* [2001] and *Saito et al.* [1995]. According to *Lessard and Knudsen* [2001], Alfvén waves with short wavelength ($\lesssim$ 1 km) are not reflected by the ionosphere. As *Lühr et al.* [2014] mainly focused on the scale sizes below 4 km, the effect of ionospheric reflection is expected not to be large. *Saito et al.* [1995] stated that Pedersen conductance in the nighttime midlatitudes is not much different from the Alfvénic conductance. Note in *Lühr et al.* [2014, Figure 8a] that most events in the study occur at |MLAT| ~10°–20°, which is not so far from the midlatitude region addressed by *Saito et al.* [1995, Figure 8]. Considering *Burke et al.* [2016a, equation (3)], hence, we may also expect perfect impedance matching and no ionospheric reflection for the EPB events in *Lühr et al.* [2014]. *E* field and *B* field variations inside EPBs (i.e., Alfvén wave signatures), as estimated from the Swarm observations, are under investigation of the GeoForschungsZentrum team and will be published in the future. Although the Swarm constellation does not provide 50 Hz *E* field data which are necessary for fully verifying the method of *Lühr et al.* [2014], the results based on 2 Hz *E* field data can partly test the validity of the assumptions used by *Lühr et al.* [2014].

4.5. Identity of $\delta\vec{E}_{\text{perp}}$ and $\delta\vec{B}_{\text{perp}}$: Do They Really Represent Alfvén Waves?

Finally, we discuss the identity of $\delta\vec{E}_{\text{perp}}$ and $\delta\vec{B}_{\text{perp}}$ measured by Swarm. One may question that the field fluctuations may not represent Alfvén waves but spatially inhomogeneous electromagnetic fields of other origins which are measured by a fast moving platform such as Swarm. At the fluctuation frequencies we consider in this paper (f; below the Nyquist frequency of 0.5 Hz), the distance d between the Swarm satellites and the reflection layer (or the order of 100 km) is assumed to be small compared to the field-aligned wavelength of the Alfven waves, $\lambda_{\parallel} = V_A/f$. According to *Lysak* [1999, Figure 2], typical V_A values near Swarm altitudes are of the order of 100 km/s, which leads to $\lambda_{\parallel}$ of the order of 1000 km. In this limit $d/\lambda_{\parallel} \ll 1$, the wave interpretation becomes equivalent to the static interpretation in which measured fluctuations are purely spatial.

For example, the ratio $|\delta\vec{E}_{perp}|/|\delta\vec{B}_{perp}| = 1/(\mu_0\Sigma_{PR})$ regardless of whether the fluctuations are spatial or temporal [*Knudsen et al.*, 1990].

In addition, good agreement of our Figures 4 and 5 with *Keiling et al.* [2003] and *Zhang et al.* [2012] also supports that a majority of $\delta\vec{E}_{perp}$ and $\delta\vec{B}_{perp}$ in our study originates from Alfvén waves. *Keiling et al.* [2003] used data from a magnetospheric satellite (Polar), and *Zhang et al.* [2012] conducted magnetohydrodynamic (MHD) simulations to obtain Alfvén wave Poynting flux. Neither the Polar satellite nor the MHD model can be severely affected by the spatial field inhomogeneities measured by a fast moving platform.

5. Summary and Conclusion

In this study we have statistically investigated Poynting flux and reflection coefficients of Alfvén waves (scale size ~10–100 km) in the high-latitude ionosphere. For that aim we analyzed the *E* field, *B* field, and plasma density data observed by Swarm-Alpha and Swarm-Bravo between December 2013 and March 2015, following the method of *Burke et al.* [2016b]. Our main conclusions can be summarized as follows:

1. At dayside regions surrounding the cusp and around nightside auroral region the ionospheric reflection coefficient is high, while it is low or even negative in the polar cap.
2. The reflection coefficient is generally higher in the summer than in the winter hemisphere.
3. In summer the dayside coefficients are generally higher than the nightside ones. In winter the coefficient exhibits weak peaks in the postmidnight sector.

Items 1–3 roughly agree with previous models for ionospheric Pedersen conductance. A number of discrepancies in the detailed distributions, which were addressed in section 4, suggest the need for further studies or reliable modeling of ionospheric Pedersen conductance.

In addition, our study revealed the following features for Poynting flux and in situ plasma density associated with the reflection coefficient distributions.

1. The Poynting flux is mainly downward in both hemispheres in all the seasons. Peak magnitudes (approaching 1 mW/m^2) appear surrounding the noontime cusp and near-midnight auroral regions. These results confirm previous magnetospheric studies [e.g., *Keiling et al.*, 2003] from the ionospheric side. The Poynting flux magnitude generally exhibits hemispheric symmetry.
2. Poynting flux estimation from $\delta\vec{B}$ data assuming freely downward propagating Alfvén waves leads to about 3 times the flux estimated from the $\delta\vec{E}$ and $\delta\vec{B}$.
3. The ionospheric reflection coefficients are not controlled by in situ electron density at Swarm altitudes. It suggests the importance of *E* region conductivity for wave reflection at the high-latitude ionosphere, as expected from previous studies such as *Juusola et al.* [2016a].

Due to the noise issues and limited coverage of the Swarm *E* field data [*Knudsen et al.*, 2014], there are caveats for the conclusions given above, which were extensively discussed in section 4. Future observations with long-term data sets as well as computer simulations are warranted to fully establish the climatological behavior of high-latitude ionospheric reflection coefficients and Poynting flux distribution.

Acknowledgments
The authors appreciate valuable discussions with C. Stolle and J. Rodriguez-Zuluaga about the Swarm/TII data usage. The European Space Agency (ESA) is acknowledged for providing the Swarm data, which are accessible at https://earth.esa.int/web/guest/swarm/data-access. JP was supported by the "Planetary system research for space exploration" project, the basic research funding from KASI, and the Air Force Research Laboratory, under agreement FA2386-14-1-4004. J.K.B. was supported by a Canadian Space Agency grant. Swarm-EFI/TII data processing and calibration is supported by the Canadian Space Agency.

References

Ahn, B.-H., A. D. Richmond, Y. Kamide, H. W. Kroehl, B. A. Emery, O. de la Beaujardière, and S.-I. Akasofu (1998), An ionospheric conductance model based on ground magnetic disturbance data, *J. Geophys. Res.*, *103*(A7), 14,769–14,780, doi:10.1029/97JA03088.

Aikio, A. T., L. Cai, and T. Nygrén (2012), Statistical distribution of height-integrated energy exchange rates in the ionosphere, *J. Geophys. Res.*, *117*, A10325, doi:10.1029/2012JA018078.

Alfvén, H. (1942), Existence of electromagnetic-hydrodynamic waves, *Nature*, *150*(3805), 405–406, doi:10.1038/150405d0.

Burke, W. J., C. R. Martinis, P. C. Lai, L. C. Gentile, C. Sullivan, and R. F. Pfaff (2016a), C/NOFS observations of electromagnetic coupling between magnetically conjugate MSTID structures, *J. Geophys. Res. Space Physics*, *121*, 2569–2582, doi:10.1002/2015JA021965.

Burke, W. J., R. F. Pfaff, C. R. Martinis, and L. C. Gentile (2016b), C/NOFS remote sensing of ionospheric reflectance, *J. Geophys. Res. Space Physics*, *121*, 4924–4932, doi:10.1002/2016JA022345.

Chaston, C. C., C. W. Carlson, J. P. McFadden, R. E. Ergun, and R. J. Strangeway (2007), How important are dispersive Alfvén waves for auroral particle acceleration?, *Geophys. Res. Lett.*, *34*, L07101, doi:10.1029/2006GL029144.

Cousins, E. D. P., T. Matsuo, and A. D. Richmond (2015), Mapping high-latitude ionospheric electrodynamics with SuperDARN and AMPERE, *J. Geophys. Res. Space Physics*, *120*, 5854–5870, doi:10.1002/2014JA020463.

Fedorov, E., N. Mazur, V. Pilipenko, and M. Engebretson (2016), Interaction of magnetospheric Alfvén waves with the ionosphere in the Pc1 frequency band, *J. Geophys. Res. Space Physics*, *121*, 321–337, doi:10.1002/2015JA021020.

Finlay, C. C., N. Olsen, S. Kotsiaros, N. Gillet, and L. Tøffner-Clausen (2016), Recent geomagnetic secular variation from Swarm and ground observatories as estimated in the CHAOS-6 geomagnetic field model, *Earth Planets Space*, *68*, 112, doi:10.1186/s40623-016-0486-1.

Fiori, R. A. D., A. V. Koustov, D. H. Boteler, D. J. Knudsen, and J. K. Burchill (2016), Calibration and assessment of Swarm ion drift measurements using a comparison with a statistical convection model, *Earth Planets Space*, *68*, 100, doi:10.1186/s40623-016-0472-7.
Green, D. L., C. L. Waters, H. Korth, B. J. Anderson, A. J. Ridley, and R. J. Barnes (2007), Technique: Large-scale ionospheric conductance estimated from combined satellite and ground-based electromagnetic data, *J. Geophys. Res.*, *112*, A05303, doi:10.1029/2006JA012069.
Haerendel, G. (2014), M-I coupling scales and energy dumping, *Geophys. Res. Lett.*, *41*, 1846–1853, doi:10.1002/2014GL059582.
Ishii, M., M. Sugiura, T. Iyemori, and J. A. Slavin (1992), Correlation between magnetic and electric field perturbations in the field-aligned current regions deduced from DE 2 observations, *J. Geophys. Res.*, *97*(A9), 13,877–13,887, doi:10.1029/92JA00110.
Juusola, L., et al. (2014), Statistical comparison of seasonal variations in the GUMICS-4 global MHD model ionosphere and measurements, *Space Weather*, *11*, 582–600, doi:10.1002/2014SW001082.
Juusola, L., K. Kauristie, H. Vanhamäki, A. Aikio, and M. van de Kamp (2016a), Comparison of auroral ionospheric and field-aligned currents derived from Swarm and ground magnetic field measurements, *J. Geophys. Res. Space Physics*, *121*, 9256–9283, doi:10.1002/2016JA022961.
Juusola, L., W. E. Archer, K. Kauristie, J. K. Burchill, H. Vanhamäki, and A. T. Aikio (2016b), Ionospheric conductances and currents of a morning-sector auroral arc from Swarm-A electric and magnetic field measurements, *Geophys. Res. Lett.*, *43*, 11,519–11,527, doi:10.1002/2016GL070248.
Keiling, A. (2009), Alfvén waves and their roles in the dynamics of the Earth's magnetotail: A review, *Space Sci. Rev.*, *142*, 73–156, doi:10.1007/s11214-008-9463-8.
Keiling, A., J. R. Wygant, C. A. Cattell, F. S. Mozer, and C. T. Russell (2003), The global morphology of wave Poynting flux: Powering the aurora, *Science*, *299*, 383–386.
Keiling, A., G. K. Parks, J. R. Wygant, J. Dombeck, F. S. Mozer, C. T. Russell, A. V. Streltsov, and W. Lotko (2005), Some properties of Alfvén waves: Observations in the tail lobes and the plasma sheet boundary layer, *J. Geophys. Res.*, *110*, A10S11, doi:10.1029/2004JA010907.
Kelley, M. C., D. J. Knudsen, and J. F. Vickrey (1991), Poynting flux measurements on a satellite: A diagnostic tool for space research, *J. Geophys. Res.*, *96*(A1), 201–207, doi:10.1029/90JA01837.
Knudsen, D. J., M. C. Kelley, G. D. Earle, J. F. Vickrey, and M. Boehm (1990), Distinguishing Alfvén waves from quasi-static field structures associated with the discrete aurora: Sounding rocket and HILAT satellite measurements, *Geophys. Res. Lett.*, *17*(7), 921–924, doi:10.1029/GL017i007p00921.
Knudsen, D. J., M. C. Kelley, and J. F. Vickrey (1992), Alfvén waves in the auroral ionosphere: A numerical model compared with measurements, *J. Geophys. Res.*, *97*(A1), 77–90, doi:10.1029/91JA02300.
Knudsen, D., J. Burchill, S. Buchert, I. Coco, L. Tøffner-Clausen, and P. E. Holmdahl Olsen (2014), Swarm preliminary Plasma dataset User Note. SWAM-GSEG-EOPG-TN-15-0003, Issue/Revision 1.0, European Space Agency (ESA). [Available at https://earth.esa.int/documents/10174/1514862/Swarm_Preliminary_Plasma_Dataset_User_Note.]
Knudsen, D. J., J. K. Burchill, S. C. Buchert, A. I. Eriksson, R. Gill, J.-E. Wahlund, L. Åhlen, M. Smith, and B. Moffat (2017), Thermal ion imagers and Langmuir probes in the Swarm electric field instruments, *J. Geophys. Res. Space Physics*, *122*, doi:10.1002/2016JA022571, in press.
Kwak, Y.-S., and A. D. Richmond (2007), An analysis of the momentum forcing in the high-latitude lower thermosphere, *J. Geophys. Res.*, *112*, A01306, doi:10.1029/2006JA011910.
Lessard, M. R., and D. J. Knudsen (2001), Ionospheric reflection of small-scale Alfvén waves, *Geophys. Res. Lett.*, *28*, 3573–3576, doi:10.1029/2000GL012529.
Li, K., et al. (2012), On the ionospheric source region of cold ion outflow, *Geophys. Res. Lett.*, *39*, L18102, doi:10.1029/2012GL053297.
Lühr, H., J. Park, C. Xiong, and J. Rauberg (2014), Alfvén wave characteristics of equatorial plasma irregularities in the ionosphere derived from CHAMP observations, *Front. Phys.*, *2*, 47, doi:10.3389/fphy.2014.00047.
Lysak, R. L. (1993), Generalized model of the ionospheric Alfvén resonator, in *Auroral Plasma Dynamics*, edited by R. L. Lysak, pp. 121–128, AGU, Washington, D. C.,10.1029/GM080p0121.
Lysak, R. L. (1999), Propagation of Alfvén waves through the ionosphere: Dependence on ionospheric parameters, *J. Geophys. Res.*, *104*(A5), 10,017–10,030, doi:10.1029/1999JA900024.
Newell, P. T., T. Sotirelis, and S. Wing (2009), Diffuse, monoenergetic, and broadband aurora: The global precipitation budget, *J. Geophys. Res.*, *114*, A09207, doi:10.1029/2009JA014326.
Olsen, N., et al. (2013), The Swarm Satellite Constellation Application and Research Facility (SCARF), *Earth Planets Space*, *65*, 1189–1200.
Park, J., H. Lühr, C. Stolle, J. Rodriguez-Zuluaga, D. J. Knudsen, J. K. Burchill, and Y.-S. Kwak (2016), Statistical survey of nighttime midlatitude magnetic fluctuations: Their source location and Poynting flux as derived from the Swarm constellation, *J. Geophys. Res. Space Physics*, *121*, 11,235–11,248, doi:10.1002/2016JA023408.
Pedatella, N, C Stolle, and J Chau (2015), Comparing Swarm electron density data to COSMIC GPS radio occultation observations, paper presented at the 26th IUGG General Assembly, The International Union of Geodesy and Geophysics (IUGG), Prague, Czech Republic, June 22–July 2.
Ridley, A. J. (2007), Effects of seasonal changes in the ionospheric conductances on magnetospheric field-aligned currents, *Geophys. Res. Lett.*, *34*, L05101, doi:10.1029/2006GL028444.
Ridley, A. J., T. I. Gombosi, and D. L. DeZeeuw (2004), Ionospheric control of the magnetosphere: Conductance, *Ann. Geophys.*, *22*, 567–584, doi:10.5194/angeo-22-567-2004.
Saito, A., T. Iyemori, M. Sugiura, N. C. Maynard, T. L. Aggson, L. H. Brace, M. Takeda, and M. Yamamoto (1995), Conjugate occurrence of the electric field fluctuations in the nighttime midlatitude ionosphere, *J. Geophys. Res.*, *100*(A11), 21,439–21,451.
Shi, R., H. Liu, A. Yoshikawa, B. Zhang, and B. Ni (2013), Coupling of electrons and inertial Alfvén waves in the topside ionosphere, *J. Geophys. Res. Space Physics*, *118*, 2903–2910, doi:10.1002/jgra.50355.
Siscoe, G. L. (1983), Solar system magnetohydrodynamics, in *Solar-Terrestrial Physics: Principles and Theoretical Foundations*, edited by R. L. Carovillano and and J. M. Forbes, pp. 11–99, D. Reidel, Dordrecht, Netherlands.
Stasiewicz, K., et al. (2000), Small scale Alfvénic structure, in the aurora, *Space Sci. Rev.*, *92*, 423–533, doi:10.1023/A:1005207202143.
Vogt, J. (2002), Alfvén wave coupling in the auroral current circuit, *Surv. Geophys.*, *23*, 335–377.
Xiong, C., C. Stolle, H. Lühr, J. Park, B. G. Fejer, and G. N. Kervalishvili (2016), Scale analysis of equatorial plasma irregularities derived from Swarm constellation, *Earth Planets Space*, *68*, 121, doi:10.1186/s40623-016-0502-5.
Zhang, B., W. Lotko, O. Brambles, P. Damiano, M. Wiltberger, and J. Lyon (2012), Magnetotail origins of auroral Alfvénic power, *J. Geophys. Res.*, *117*, A09205, doi:10.1029/2012JA017680.
Zhu, L., J. J. Sojka, R. W. Schunk, and D. J. Crain (1993), Influence of horizontal inhomogeneity in the ionosphere on the reflection of Alfvén waves, *Geophys. Res. Lett.*, *20*(4), 313–316, doi:10.1029/93GL00079.